Biofabrication of advanced *in vitro* 3D models to study ischaemic and doxorubicin-induced myocardial damage

Biofabrication

PAPER

Biofabrication of advanced *in vitro* 3D models to study ischaemic and doxorubicin-induced myocardial damage

Poonam Sharma[1,2,3,4], **Clara Liu Chung Ming**[4], **Xiaowei Wang**[5,6,7], **Laura A Bienvenu**[5,7], **Dominik Beck**[4], **Gemma Figtree**[2,3], **Andrew Boyle**[1] and **Carmine Gentile**[2,3,4,*]

[1] The University of Newcastle, Newcastle, NSW 2308, Australia
[2] University of Sydney, Sydney, NSW 2000, Australia
[3] Kolling Institute of Medical Research, Royal North Shore Hospital, Sydney, NSW 2065, Australia
[4] University of Technology, Sydney, NSW 2007, Australia
[5] Molecular Imaging and Theranostics Laboratory, Baker Heart and Diabetes Institute, Melbourne, VIC 3004, Australia
[6] Monash University, Melbourne, , VIC 3800, Australia
[7] University of Melbourne, Melbourne, VIC 3010, Australia
[*] Author to whom any correspondence should be addressed.

E-mail: carmine.gentile@uts.edu.au

Keywords: *in vitro* advanced cardiac models, myocardial infarction, reperfusion injury, cardiac spheroids, I/R

Supplementary material for this article is available online

OPEN ACCESS

RECEIVED
1 December 2021

ACCEPTED FOR PUBLICATION
4 January 2022

PUBLISHED
24 January 2022

Abstract

Current preclinical *in vitro* and *in vivo* models of cardiac injury typical of myocardial infarction (MI, or heart attack) and drug induced cardiotoxicity mimic only a few aspects of these complex scenarios. This leads to a poor translation of findings from the bench to the bedside. In this study, we biofabricated for the first time advanced *in vitro* models of MI and doxorubicin (DOX) induced injury by exposing cardiac spheroids (CSs) to pathophysiological changes in oxygen (O_2) levels or DOX treatment. Then, contractile function and cell death was analyzed in CSs in control verses I/R and DOX CSs. For a deeper dig into cell death analysis, 3D rendering analyses and mRNA level changes of cardiac damage-related genes were compared in control verses I/R and DOX CSs. Overall, *in vitro* CSs recapitulated major features typical of the *in vivo* MI and drug induced cardiac damages, such as adapting intracellular alterations to O_2 concentration changes and incubation with cardiotoxic drug, mimicking the contraction frequency and fractional shortening and changes in mRNA expression levels for genes regulating sarcomere structure, calcium transport, cell cycle, cardiac remodelling and signal transduction. Taken together, our study supports the use of I/R and DOX CSs as advanced *in vitro* models to study MI and DOX-induced cardiac damge by recapitulating their complex *in vivo* scenario.

1. Introduction

Cardiovascular disease (CVD) (including myocardial infarction (MI) and drug-induced cardiotoxicity) is the major cause of death worldwide [1, 2]. MI is characterized by prolonged ischaemia (on average longer than 20 min) due to the blockage of coronary arteries causing cardiac cell death, inflammatory response, fibroblast infiltration and fibrosis [3]. Prompt myocardial reperfusion is necessary to maintain a healthy and functional ischaemic myocardium following an MI event [4]. However, restoration of blood flow following ischaemia is characterized by the release of high oxygen-led toxic compounds to the myocardium, including reactive oxygen (O_2) and nitrogen species, known as myocardial 'ischaemia/reperfusion (I/R) injury' [5]. Cancer is the largest killer globally [6]. The current therapies using doxorubicin (DOX) which is a widely used anticancer drug for leukemia, lymphoma and breast cancer patients, is related to delayed cardiotoxic effects in these patients (up to 17 years following their treatment). While several mechanisms have been identified for DOX-induced myocardial damage, including cell-specific effects in *in vitro* cardiac spheroids (CSs), its complex scenario is poorly recapitulated

in currently available *in vitro* models using human cardiac cells in monolayer cultures [7, 8]. As a consequence, there is a lack of thorough understanding of the mechanisms regulating myocardial damage following I/R injury and DOX treatment, and a limited translation of findings from the bench to the bedside, with serious consequences for CVD patients [9].

One of the primary reasons for the poor translation of currently used *in vitro* models for cardiovascular research is their limited recapitulation of the *in vivo* heart microenvironment and pathophysiology [10, 11]. In order to overcome this, advanced *in vitro* pathophysiological models of the human heart employing 3D cultures of cardiac cells have recently emerged [2, 12–14]. These include human cardiac organoids and 3D cultures of cardiac cells grown in a bioreactor, used to model MI and drug induced cardiotoxicity cues, such as a gradient for O_2 and nutrient and extracellular matrix deposition closer to the *in vivo* heart microenvironment [15]. Mimicking *in vivo*-like MI conditions is critical for the optimal *in vitro* modeling of myocardial damage. In the case of ischaemic damage, it is crucial to consider the concentration of O_2 required to generate pathophysiological hypoxia and reoxygenation in *in vivo* conditions, which may differ *in vitro*. Physiological O_2 concentration in the heart ranges between 3% and 5% *in vivo*, whereas most *in vitro* cardiac models are exposed to 20% O_2 in the incubator [16]. These are critical considerations for the recapitulation of the pathophysiology typical of an MI event. In case of drug-induced myocardial damage, the concentration of the drug is dependent on the thickness and the presence of cellular-extracellular components that make up the 3D cardiac microenviroment [8, 17, 18]. Our previous studies showed that *in vitro* 3D human cardiac spheroids (hCSs) better recapitulate the heart microenvironment by their comparison with *ex vivo* human heart biopsies [8]. Similarly, CSs have been generated from rodent cells as well [19]. CSs are generated by co-culturing cardiac endothelial cells, myocytes and fibroblasts at ratios found in the human heart and present morphological, biochemical and pathophysiological features typical of the *in vivo* microenvironment. Based on their unique features to better recapitulate the human heart microenvironment, they have been used to test toxicity of DOX and to model cardiac fibrosis *in vitro,* which is the stiffening of the heart typical of myocardial damage [8, 19]. While other studies attempted at recapitulating cardiac fibrosis *in vitro* as well, this has been successfully modelled in CSs by exposing them to TGF-beta 1 and DOX [19]. Therefore, the hypothesis of this study is that CSs can be used as advanced *in vitro* models to study myocardial injury typical of an *in vivo* MI event, as well as following DOX-treatment.

2. Material and methods

2.1. Mouse cardiac cell isolation and generation of mouse cardiac spheroids (mCSs)

Neonatal cardiac cells were isolated from mice between the age of one and five days. Neonatal mouse hearts were isolated following protocol approval from the Animal Ethics Committee at the Northern Sydney Local Health District (St Leonards, NSW, Australia). Briefly, murine hearts were isolated from one to five-day old mice, then chopped into smaller pieces and enzymatically digested with the Miltenyi Biotech GentleMACS dissociator. Single cells were then isolated using a 0.2-micron cell strainer on top of the 50 ml tube. The enzyme reaction is blocked by adding complete DMEM, containing 10% (v/v) FBS + 1% (v/v) pen/strep + 1%(v/v) L-glutamine, centrifuged at 300 g, for 5 min at 4 °C. Cell pellet thus obtained is resuspended into complete DMEM. CSs were generated by co-culturing 30 000 mice cardiac cells (immediately after their isolation) in 15 μl hanging drop cultures containing complete DMEM, using Perfecta 3D® 384-well hanging drop plates (3D Biomatrix, Ann Arbor, MI, USA) (figure 1). Media was replaced every 2–3 d.

2.2. Generation of human cardiac spheroids (hCSs)

hCSs were generated according to our previously published protocol [18]. Briefly, human induced pluripotent stem cell-derived cardiomyocytes (hiPSCs-CMs) (iCells, Fujifilm Cellular Dynamics, Inc.) were cultured in fibronectin pre-coated culture flasks following the manufacturer's instruction manual. HiPSCs-CMs were then isolated from culture flasks and mixed with primary human cardiac fibroblasts (HCFs) (Cell Applications, San Diego, CA, USA) and primary human coronary artery endothelial cells (Cell Applications, San Diego, CA, USA) in 2:1:1 ratio by plating 10 000 hiPSCs-CMs, 5000 HCFs and 5000 HCAECs per hanging drop culture containing 20 μl of CS medium into each well of the 384 well HDC. HCS media was prepared by mixing iCells Maintenance Medium, Human Cardiac Fibroblast Medium and Meso Endo Growth Medium in 2:1:1 ratio. HCS media was replaced every 2–3 d (figure 1).

2.3. *In vivo* mouse myocardial I/R injury

Left ventricular specimens of adult mice that have undergone myocardial I/R injury were kindly donated for mRNA isolation by A/Prof Xiaowei Wang (Molecular Imaging and Theranostics Laboratory, Baker Heart and Diabetes Institute, Melbourne, Australia). Briefly, adult male mice (6 weeks old) were divided into the following groups: (a) control (no injury); and (b) ischaemia/reperfusion (I/R) injury. I/R injury was induced by endoluminal occlusion of the left anterior descending (LAD) coronary

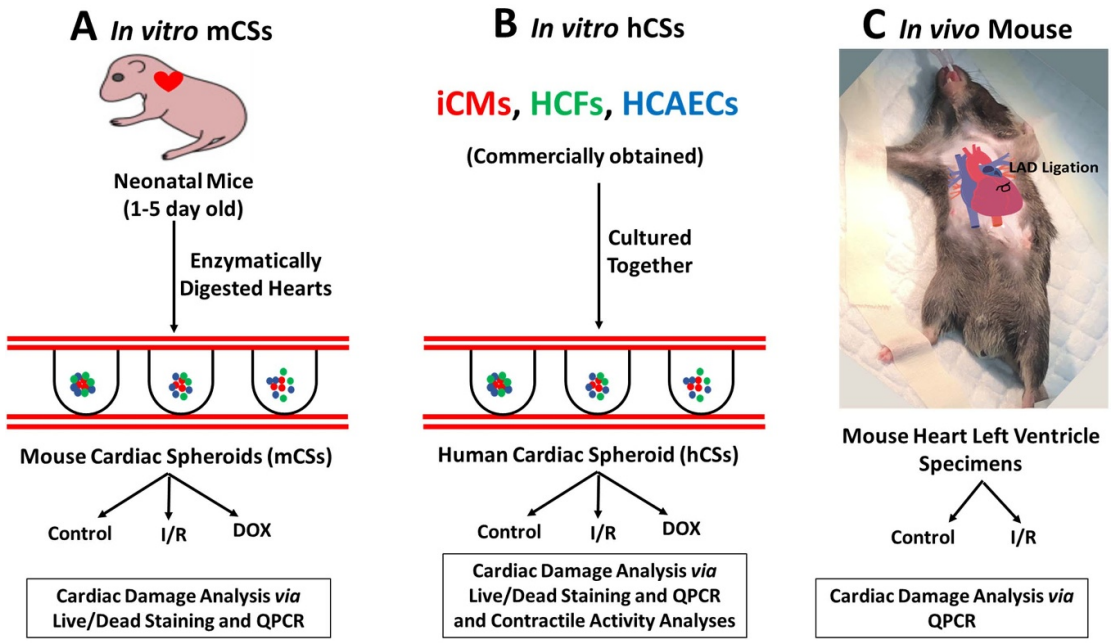

Figure 1. Protocol for *in vitro* and *in vivo* myocardial damage models used in this study. A schematic representing the procedures and analyses performed for I/R injury and DOX-induction in *in vitro* mCSs (A) and hCSs (B), and for *in vivo* I/R injury in adult mouse (C).

artery for 60 min, followed by reperfusion and recovery (figure 1). Hearts were collected 3 d later [20, 21]. Cellular damage was evaluated by qPCR analysis described above and compared with *in vitro* studies.

2.4. Establishment of the myocardial I/R injury in CSs using EVOS FL auto system

In vitro modeling of the hypoxic/normoxic-driven cardiac damage was achieved by culturing CSs at varying oxygen concentrations while evaluating changes in intracellular O_2 concentrations in a live imaging system (EVOS FL Auto system, Life Technologies). First, Image-iT (a reversible hypoxic fluorescent dye sensible to changes in intracellular O_2 levels, Thermo Fisher Scientific,AU) was added to CSs. Then, labeled CSs were moved to the live imaging gas chamber where they were cultured at 5% O_2 for 24 h to mimic *in vivo* normoxic conditions. To mimic the hypoxia typical of the ischemic event, CSs were then exposed to hypoxic conditions (0% O_2) for 20 h Reoxygenation of CSs was performed by increasing the O_2 concentrations again to 5% from T20 to T37.

2.5. Doxorubicin-mediated toxicity in CSs

HCSs were treated with 10 μM DOX (based on the previously established protocol for cell death in CSs) and incubated for 18 h at 37 °C, 5% CO_2 [8, 18]. Control hCSs contained media without any DOX. After 18 h of treatment, hCSs were evaluated for cellular damage and contractile function.

2.6. Cell viability and death analyses

Cell viability and death were evaluated by incubating CSs with calcein-AM and ethidium homodimer (staining live and dead cells, respectively) as previously described (Invitrogen LIVE/DEAD Viability/Cytotoxicity Kit) [8, 17]. Nuclei were stained with Hoechst stain. Stained CSs were imaged using a Zeiss LSM 800 Laser Confocal Microscope (Carl Zeiss AG, Oberkochen, Germany). Optical sectioning along the *Z* axis was performed, and the images collapsed into a single focal plane using the manufacturer's software. Images were processed using Adobe Photoshop CC (Adobe Systems, Inc., San Jose, CA) and NIH ImageJ software to obtain black and white ratios of the CSs, which were then used for fluorescence quantification.

2.7. CS staining, confocal imaging and 3D rendering analyses

CSs were first stained for ethidium homodimer, fixed with 4% paraformaldehyde for an hour at room temperature, permeabilized in PBS/0.01% sodium azide (PBSA) containing 0.02% Triton-X-100 for 60 min, blocked with a 3% bovine serum albumin/PBSA solution, and then incubated with appropriate primary (15 μg ml^{-1}) and secondary (10 μg ml^{-1}) antibodies at 4 °C (18 h). Endothelial cells were identified by immunostaining for CD31 with primary mouse anti-human CD31 (BD Pharmingen, San Diego, CA, USA) and secondary Cy3-conjugated donkey anti-mouse (Jackson Immunological Research Laboratories) antibodies, based on previously established protocols. CSs were also stained with mouse monoclonal

[1C11] anti-human cardiac troponin T and mouse monoclonal [V9] to vimentin (Alexa 488) antibodies.

Confocal imaging was performed on stained CSs using a Leica Stellaris WL confocal imaging system. Images were processed using NIH Fiji software and Adobe Photoshop 2021 (Adobe Systems, In., San Jose, CA, USA). For 3D rendering analyses, confocal images of stained CSs were processed using Imaris v 9.2 software (Bitplane, Concord, MA, USA).

2.8. Fractional shortening and contractile frequency measurements

Human CS movements ($n > 8$ for each condition) were analyzed using an Olympus microscope and the contractility of each CS was recorded using Olympus Cellsens software. The fractional shortening percentage and the frequency of contractions for each CS was measured for I/R versus control and DOX versus control, respectively. This was done, by measuring the total number of contractions of the CS, and by measuring the total length of each CS through the CS contractility/movement for each video.

2.9. mRNA isolation and qPCR analyses

Isolation of mRNA from CSs was performed using RNeasy Plus Mini Kit (Qiagen) following the manufacturer's guidelines. mRNA quality was measured using a Nanodrop device. Reverse transcription was performed on the mRNA obtained using RT2 First Strand Kit, and the resulting cDNA (20 μl) was diluted with 91 μl of water and used as polymerase chain reaction (PCR) template. Diluted cDNA was then mixed with 2 $\times$ RT2 SYBR Green Mastermix (Qiagen) and water and then transferred on the mouse and human CVD PCR array (PAMM-174Z and PAHS-174Z, Qiagen). qPCR analysis was performed using Quantstudio 12 K Flex PCR machine with a 384 block. Ct values were exported and analyzed using Qiagen web-based analysis tools. Four biological repeats were used.

The normalized differentially expressed fold change values (log2 fold change $\geqslant |1|$, adjusted $P < 0.05$) of all the genes of the array obtained from Qiagen web-based analysis were used to perform principal component analysis (PCA) to produce an unsupervised hierarchical clustering heat map in Partek Genomics Suite software (version 7.0) (Partek Inc., St. Louis, MO, USA).

2.10. Statistical analysis

Data were analyzed using Graphpad Prism software to calculate mean $\pm$ standard deviation (SD) and perform appropriate unpaired t-test according to distribution and sample variance. One-way ANOVA with Tukey post-hoc test was used for comparisons of multiple groups. Significance was set to $p < 0.05$. For single gene expression analysis, fold changes were calculated as $2^{\wedge}(-\text{Avg.}\Delta\Delta Ct)$ and analyzed based on the online software from Qiagen. A minimum of $n = 3$ biological replicates was used per group.

3. Results

3.1. Establishment of I/R injury in *in vitro* CSs

CSs stained with reversible hypoxic fluorescent dye were analyzed by assessing the overtime change in fluorescence intensity following the changes in intracellular O_2 concentration. An increase in the fluorescence intensity was observed when CSs were exposed to hypoxic conditions (0% O_2) for 20 h (T1-T20) following the exposure to 5% O_2 for 24 h (T0). A decrease in fluorescence intensity was observed after switching the O_2 concentration back to physiological levels (5%) for 17 h (T21-37) (figure 2(A)). Our quantification of the Image-iT fluorescence was statistically significant between T0, T20 and T37, confirming a change in intracellular O_2 levels in our model (figure 2(B)).

3.2. Increased cell death in I/R and DOX CSs

To quantify the extent of loss in cell viability in CSs, toxicity ratios were calculated by measuring the fluorescence between dead and live cells figures 3(A)–(P)). Our statistical analyses of toxicity ratios between control and I/R CSs from either mouse or human origin (mCSs and hCS, respectively) confirmed a statistically significant increase in cell death in I/R conditions compared to control (figures 3(Q) and (R)).

DOX-treated hCSs were also incubated with calcein-AM, ethidium homodimer and Hoechst stain to measure the toxicity ratio (figures 4(A)–(H)). Similar to what we have observed in I/R CSs, DOX significantly increased the toxicity ratio compared to control cultures (figure 4(I)).

3.3. Cardiac cell types were differently affected by I/R- and DOX-induced damage as shown by confocal microscopy analyses

In order to evaluate which cells died following I/R conditions, hCSs were incubated with ethidium homodimer, and cell type-specific antibodies against CD31, cTNT and vimentim (staining cardiac endothelial cells, myocytes and fibroblasts, respectively). Our 3D rendering analyses of confocal microscopy images from I/R hCS showed that most of the cardiomyocytes died following I/R injury, whereas endothelial cells and fibroblasts would partially die (figures 5(A)–(H), videos 1 and 2 available online at stacks.iop.org/BF/14/025003/mmedia).

3D rendering analyses of DOX-treated hCSs analyzed in a similar way showed that cardiomyocytes were more susceptible to DOX-induced cell death in comparison to fibroblasts and endothelial cells, but not all of them would die (figures 6(A)–(G), video 1 and 3).

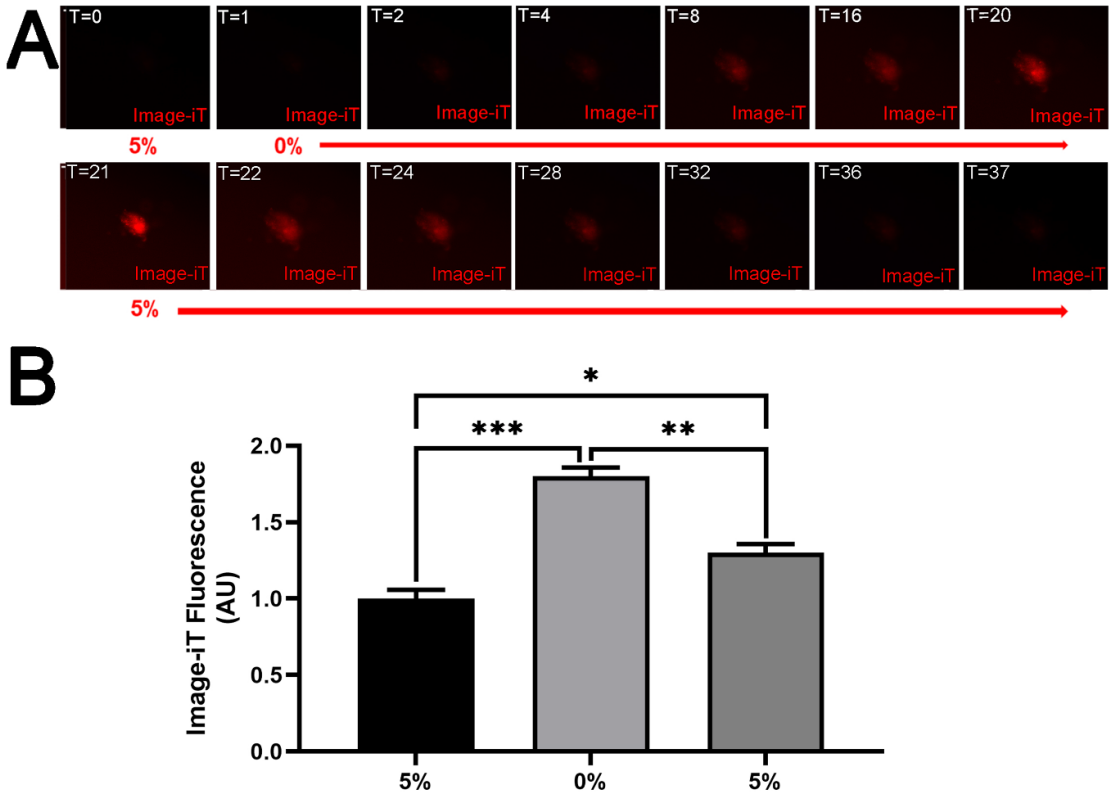

Figure 2. Intracellular O_2 concentration changes in I/R CSs. (A) Epifluorescence images of a representative CS treated with Image-iT (red) that was pre-incubated at 5% O2 ($T = 0$), and then exposed to 0% O2 for 20 h ($T = 20$) and 5% O_2 for additional 17 h ($T = 37$). (B) Statistical analysis of changes in Image-iT fluorescence between 5% ($T = 0$), 0% ($T = 20$) and 5% ($T = 37$). One-way ANOVA with Tukey post-hoc test was used for comparison of all groups. $p<0.01 = **$ and $p<0.001 = ***$. Error bars represent the mean ± SD ($n = 3$).

3.4. Decreased contraction frequency and fractional shortening in CSs following I/R injury and DOX-treatment

To evaluate the contractile activity of the hCSs following the I/R and DOX treatment, we assessed the changes in contraction frequency and fractional shortening of hCSs. We observed that while control hCS showed approximately 40 contractions per minute, I/R hCSs stopped contracting (figure 7(A)). Similarly, fractional shortening was only observed in control hCSs (figure 7(B)). Overall, it was observed a complete cessation in contractile activity in hCSs following an I/R injury (figures 7(A) and (B), videos 4 and 5).

DOX-treated CSs showed a significant decrease in contractile function and fractional shortening compared with control CSs. However, DOX CSs did not lose their contraction frequency and fractional shortening completely (figures 7(A) and (B), videos 4 and 6).

3.5. Changes in relative expression of cardiovascular genes during I/R and DOX-induced myocardial damage

To further evaluate whether *in vitro* I/R CSs mimic changes in mRNA expression levels typical of the *in vivo* I/R injury, we compared changes of cardiac damage-related genes (table 1) [22, 23]. The fold change values of all the genes from both human (*in vitro*) and mouse (*in vivo/in vitro*) CVD array was used to perform PCA. The heat maps obtained from PCA support that *in vitro* hCSs better mimic the *in vivo* I/R injury in comparison to *in vitro* mCSs (figure 8, supplementary figures 1–7).

DOX-treated CSs were analyzed for gene expression of cardiac damage-related genes via qPCR. Our PCA demonstrates that both DOX CSs (mCSs and hCSs) showed diference in gene expressions compared to I/R CSs (mCSs and hCSs) (figures 9 and 10, table 2, supplementary figures 8–14). However, it is important to further identify differences between gene families as well, as detailed below.

3.5.1. Sarcomeric genes were consistently regulated following an I/R injury and DOX treatment

Sarcomeric proteins control cardiac cell function and their expression levels change following I/R injury [24–27]. Our statistical analysis showed a similar trend in mRNA expression levels following injury in *in vivo* and *in vitro* In particular, actin alpha cardiac muscle 1 (Actc1), myosin heavy chain 6 (Myh6, cardiac muscle specific), cardiac troponin I (Tnni3), cardiac troponin T2 (Tnnt2) were all significantly downregulated in I/R CSs for both human

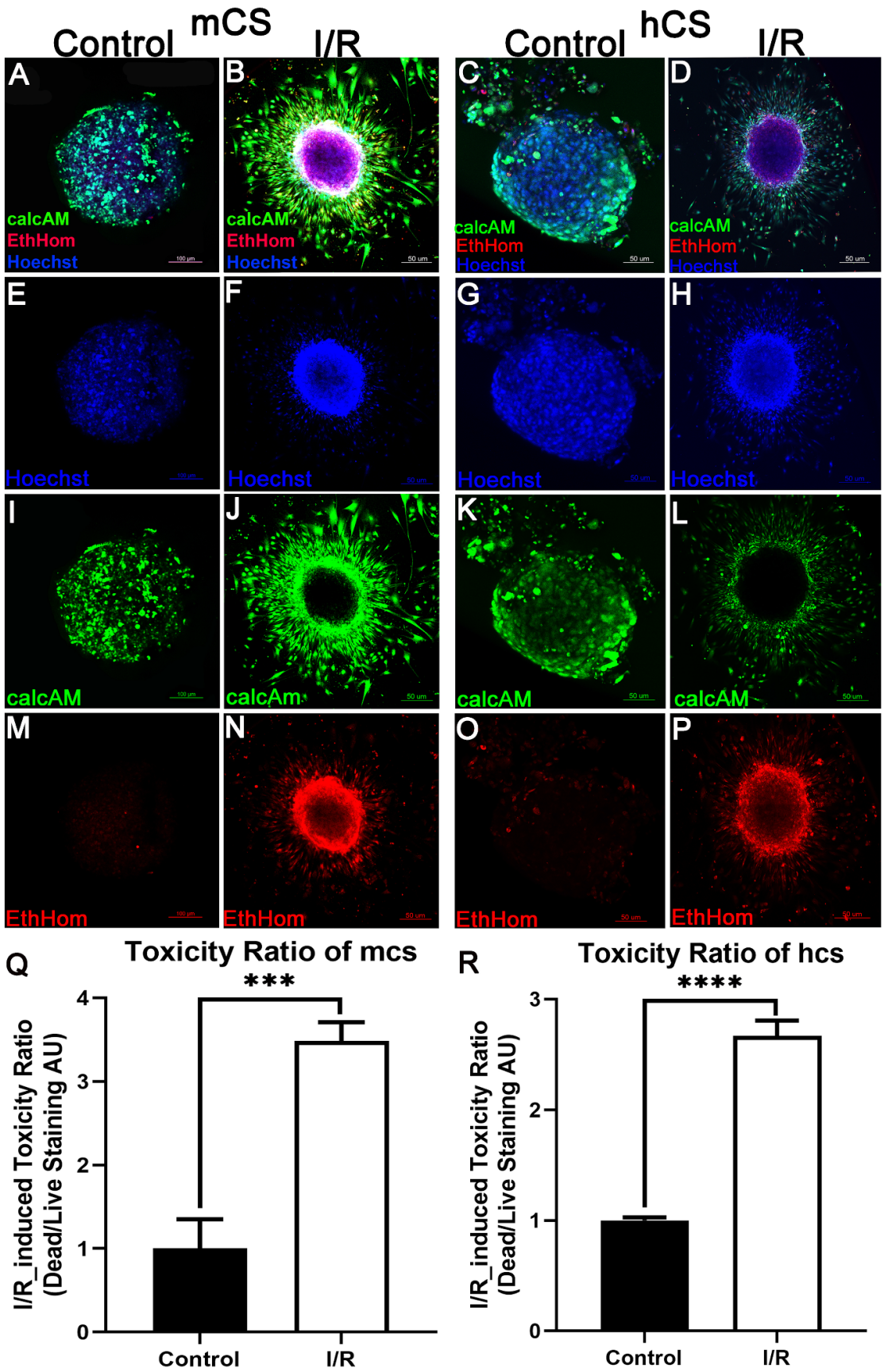

Figure 3. Confocal imaging analyses for cell death and viability in I/R CSs. (A)–(P) Collapsed z-stacks of laser scanning confocal images of control and I/R mCSs and hCSs stained with calcein-AM (green), ethidium homodimer (red) and Hoechst stain (blue), staining live, dead, and total cells, respectively. (A), (B), (C) and (D) overlays of Hoechst (E), (F), (G) and (H), calcein- AM (I), (J), (K) and (L) and ethidium homodimer (M), (N), (O) and (P) collapsed Z-stacks of control and I/R CSs. (Q) and (R) Statistical analyses of toxicity ratios for control and I/R mCSs (Q) and hCSs (R) using unpaired t-test. $p<0.001 = ***$ and $p < 0.0001 = ****$. Error bars represent the mean ± SD for $n = 3$.

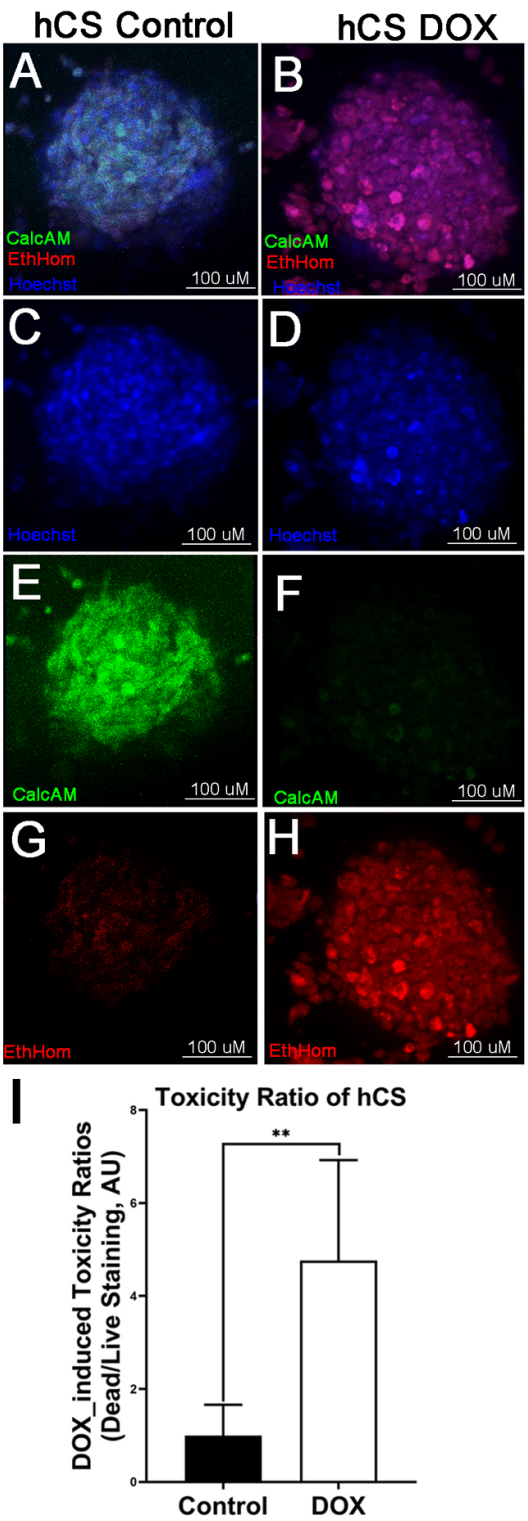

Figure 4. Confocal imaging analyses for cell death and viability in DOX CSs. (A)–(H) Collapsed z-stacks of laser scanning confocal images of control and DOX hCSs stained with calcein-AM (green), ethidium homodimer (red) and Hoechst stain (blue), staining live, dead, and total cells, respectively. (A), and (E) overlays of Hoechst (B) and (F), calcein-AM (C) and (G) and ethidium homodimer (D) and (H) collapsed Z-stacks of control and DOX CSs. (I) Statistical analyses of toxicity ratios for control and DOX hCSs using unpaired t-test. $p < 0.001 = ***$ and $p < 0.0001 = ****$. Error bars represent the mean ± SD for $n = 6$.

and murine origin when compared to control. This trend was similar to the changes measured in the *in vivo* mouse model. Similarly, myosin heavy chain 10 non-muscle (Myh10) was upregulated in both *in vitro* and *in vivo* I/R injury models (table 1).

Our statistical analysis of mRNA expression levels following DOX treatment in *in vitro* CSs showed that Actc1, Tnni3, Tnnt2 were significantly downregulated in CSs from either human or murine origin compared to control, except for Myh6 (not significant in case of hCSs). While Myh10 was significantly upregulated in both conditions compared to control, similar to what observed in our I/R injury model and constiistent with previous studies focusing on dysfunction of sarcomeric proteins post DOX-exposure (table 2) [28–30].

3.5.2. Calcium ion transport genes were downregulated in I/R and DOX CSs

Calcium ion transport genes, such as ATPase, Ca^{2+} transporting, cardiac muscle, slow twitch 2 (Atp2a2) and ATP synthase, H^+ transporting, mitochondrial F1 complex, alpha subunit 1 (Atp5a1) regulate contractile activity in cardiac myocytes [31, 32]. Both Atp2a2 and Atp5a1 were significantly downregulated in *in vivo* and *in vitro* I/R injury models compared to control, consistent with the ATP deficiency that follows an MI event (table 1) [32, 33].

Atp2a2 and Atp5a1 were significantly downregulated following DOX treatment in both mCSs and hCSs compared to controls (table 2). A similar response on calcium transporting genes was previously showed in rats during DOX treatment [34].

3.5.3. I/R injury and DOX-treatment induces overexpression of cell cycle genes

Infarcted heart tissues present a change in the expression of cell cycle controlling genes, including cyclin D1 (Ccnd1) and retinoic acid receptor responder (Rarres1) [35]. In our CS model, these two cell cycle regulatory genes were significantly upregulated in *in vivo* and *in vitro* compared to controls (table 1).

Our gene expression analysis of Ccnd1 and Rarres1 following DOX treatment showed that they were significantly upregulated in mCSs and hCSs compared to controls (table 2). These results are consistent with previous studies reporting the DOX-mediated overexpression of both genes in adult mice hearts and zebrafish [36, 37].

3.5.4. Cardiac remodeling genes were upregulated following I/R injury and DOX-treatment

In *in vivo* I/R injury models, infarcted myocardial tissue goes through extensive cardiac remodeling [38]. In our model, angiotensin-I-converting enzyme (Ace), matrix metallopeptidase 13 (Mmp13)

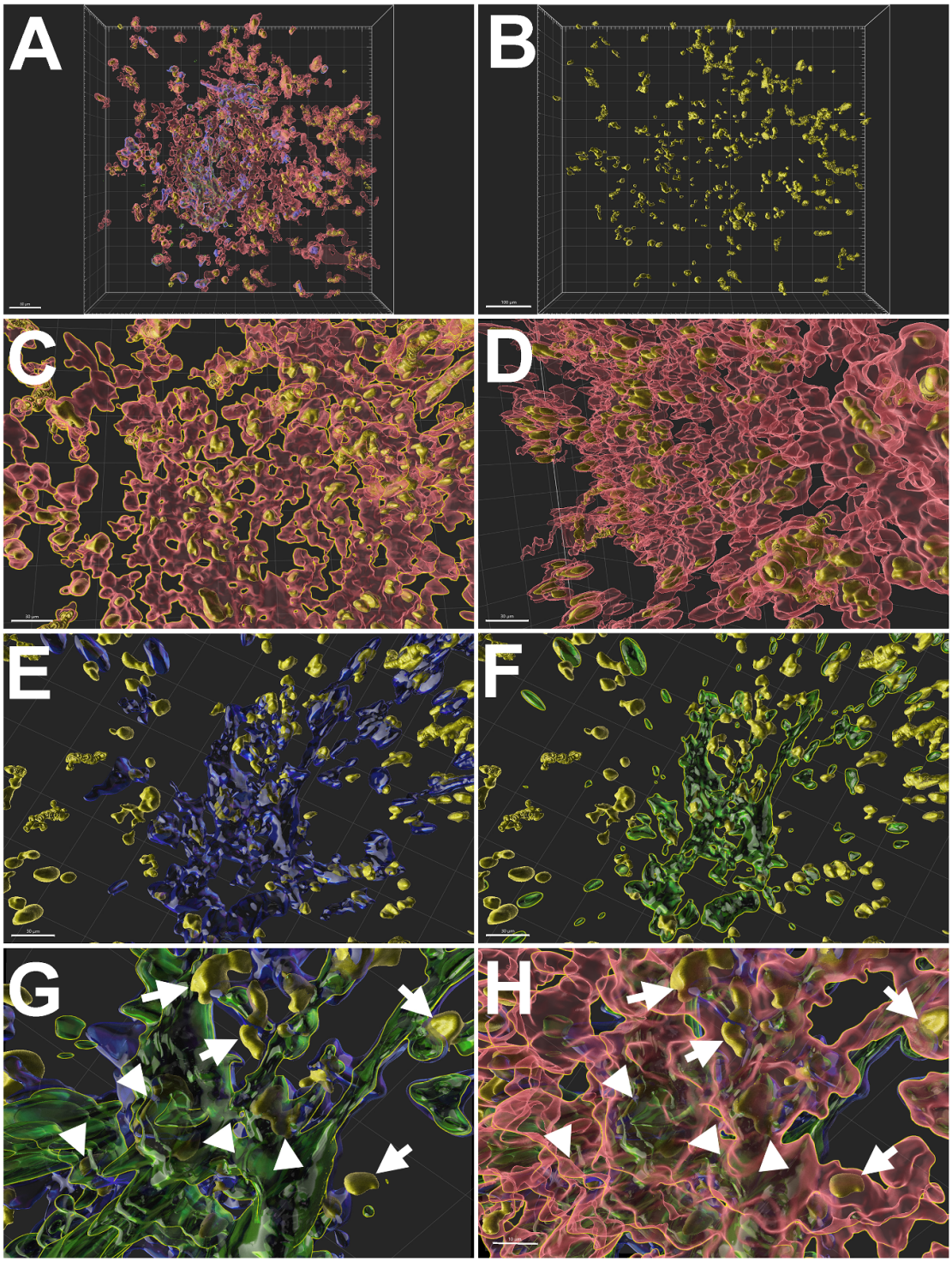

Figure 5. 3D cell death analyses of confocal images of an I/R CS using Imaris software. Confocal images of an I/R CS stained with ethidium homodimer (golden), and with antibodies against CD31 for endothelial cells (blue), cTNT for cardiomyocytes (red) and vimentim for fibroblasts (green), optimised under Imaris software. (A) and (B) shows the frontal overview of (C) and (D) highlighting all the dead cardiomyocytes. Images (E) and (F) are highlighting dead endothelial cells and fibroblasts, respectively. (G) and (H) shows the arrows point at nuclei of dead cardiomyocytes, and arrowheads to nuclei of dead endothelial cells and fibroblasts.

and renin 1 structural (Ren1) were upregulated in both *in vivo* and *in vitro* compared to control (table 1).

Ace, Mmp13 and Ren1 were similarly upregulated following DOX-mediated damaged. They all were upregulated in both mCSs and hCSs compared to control and were consistent with our I/R injury model and previous DOX mediated cardiac damage studies (table 2) [30, 39, 40].

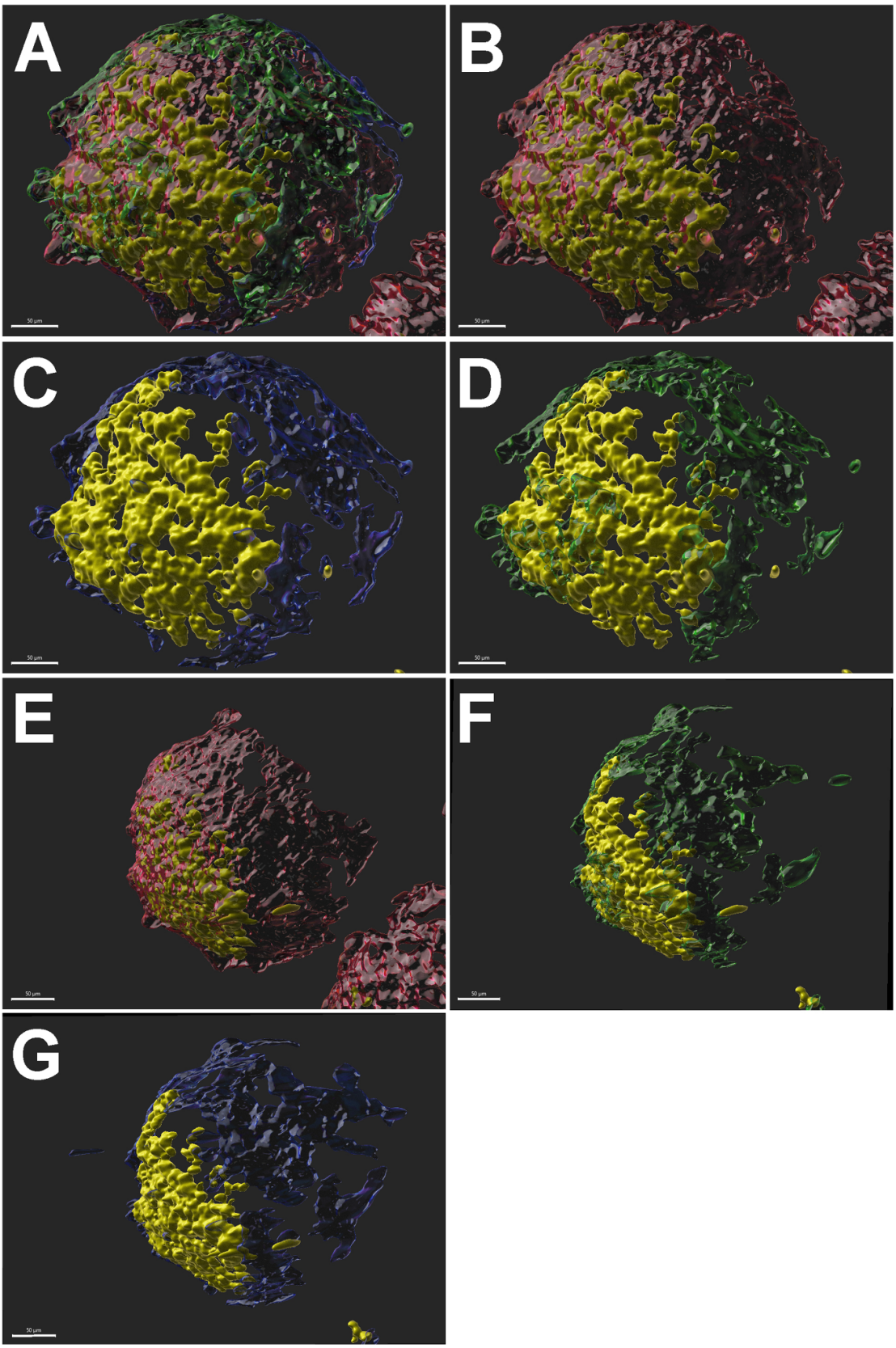

Figure 6. 3D cell death analyses of confocal images of a DOX CS using Imaris software. Confocal images of a DOX CS stained with ethidium homodimer (golden), and with antibodies against CD31 for endothelial cells (blue), cTNT for cardiomyocytes (red) and vimentim for fibroblasts (green), optimised under Imaris software. Image (A) is the overlay of (B), (C) and (D) which showed the frontal view highlighting all the dead cardiomyocytes, endothelial cells, and fibroblasts, respectively. (E), (F) and (G) images showed sideview of CS showing dead cardiomyocytes, fibroblasts, and endothelial cells respectively.

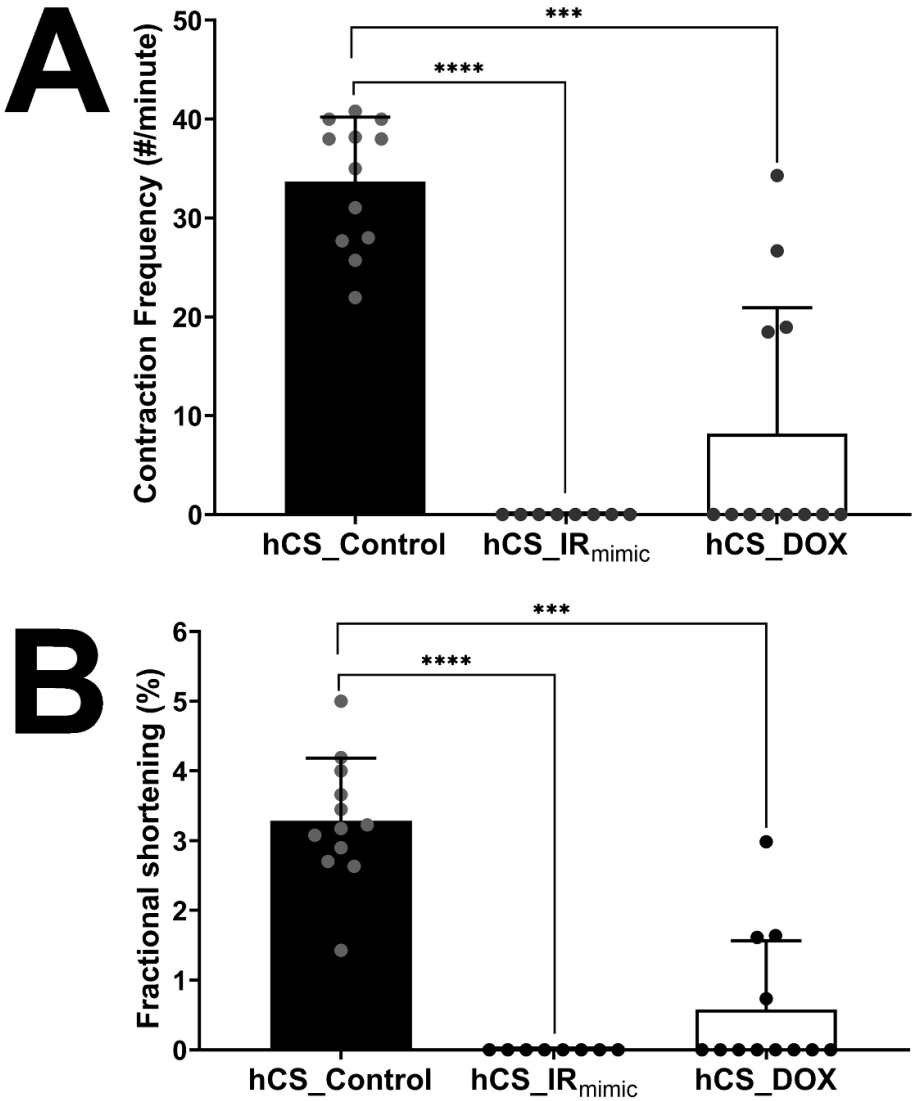

Figure 7. Decrease in contraction frequency and fractional shortening of CSs. Statistical analysis of contractile frequency (A) and fractional shortening (B) of hCSs optimized under Olympus microscope. One-way ANOVA with Tukey post-hoc test was used for comparison of all groups, $p > 0.05$ = ns, $p < 0.05$ = *, $p < 0.01$ = **, $p < 0.001$ = *** and $p < 0.0001$ = ****. Error bars represent the mean ± SD ($n > 8$).

3.5.5. Apoptosis regulating genes were differentially regulated in I/R and DOX CSs

As cell death follows an MI event, several apoptotic genes change following I/R injury *in vivo* [41]. Our qPCR analysis showed a similar trend *in vitro* and *in vivo* models for annexin A4 (Anxa4), chemokine (C-C motif) ligand (Ccl2), monoamine oxidase A (Maoa), natriuretic peptide receptor 1 (Npr1), phosphodiesterase 3 A cGMP inhibited (Pde3a) and synuclein alpha (Snca). However, natriuretic peptide type A (Nppa) and natriuretic peptide type B (Nppb) were differentially regulated in *in vivo* and *in vitro* models. Nppa and Nppb were upregulated following myocardial I/R injury in *in vivo* and *in vitro* (table 1). The differential response of Nppa and Nppb seen in *in vivo* and *in vitro* models of our study could be linked to the fact that in *in vivo* there are several additional factors that influence the disease progression other than the confounding cell types we have in our *in vitro* CS models [36, 42]. Moreover the time difference is critical for genes to respond to a stimulus, and we have different time slots for *in vivo* and *in vitro* models. The difference in both types of CSs could be species specific as one is sourced from mouse and other from human cells [43].

In mCSs all apoptotic genes (such as, Anxa4, Ccl2, Maoa, Npr1, Nppa, Nppb, Pde3a and Snca) were significantly upregulated compared to controls. However, in hCSs, Anxa4, Ccl2, Maoa, Npr1, Pde3a and Snca were upregulated, whereas Nppa and Nppb downregulated compared to control (table 2). The differential expression of Nppa and Nppb in hCSs following DOX treatment could be related to the fact that increase in their expression could be observed after 4 weeks as suggested by Boucek *et al* in 1999 while studying persistent effect of DOX on expression of cardiac genes [30].

Table 1. Expression of cardiovascular genes following I/R injury. Relative expression of sacromeric genes, calcium transporting genes, cell cycles genes, apoptotic genes, fibrotic genes and signal transduction genes in *in vivo* and *in vitro* mCSs, and *in vitro* hCSs. The blue colour represents downregulated genes and red represents the upregulated genes. Unpaired t-test, $p > 0.05$ = ns, $p<0.05$ = *, $p < 0.01$ = **, $p < 0.001$ = *** and $p < 0.0001$ = ****, ($n = 4$).

	QPCR analyses of cardiovascular genes for I/R injury evaluation					
		In vivo mouse		*In vitro* mCSs		*In vitro* hCSs	
Classification of genes	Genes	Fold change	*P*-value	Fold change	*P*-value	Fold change	*P*-value
Sarcomeric Genes	Actc1	0.137942	***	0.04	*	0.42	**
	Myh10	2.443794	***	2.08	**	5.3167	****
	Myh6	0.167832	**	0.04	**	0.44	ns
	Tnni3	0.248503	**	0.17	****	0.56	ns
	Tnnt2	0.041484	****	0.08	**	0.1	**
Calcium Transporting Genes	Atp2a2	0.168072	***	0.08	**	0.43	**
	Atp5a1	0.048586	***	0.22	****	0.5047	*
Cell Cycle Genes	Ccnd1	2.413644	***	3.37	*	3.52	***
	Rarres1	2.866099	**	16.44	****	1.46	ns
Cardiac Remodelling Genes	Ace	3.21338	****	4.43	***	1.16	ns
	Mmp13	2.571323	***	2.68	**	2.0766	*
	Ren1	2.863292	****	23.9	****	7.4	****
Apoptotic Genes	Anxa4	2.651639	****	5.54	****	1.6567	ns
	Ccl2	2.834338	**	1.97	**	1.848	*
	Maoa	2.52	***	22.14	****	1.93	ns
	Nppa	5.938162	****	0.07	ns	0.09	*
	Nppb	0.496905	ns	13.57	****	0.28	*
	Npr1	2.529959	***	21.83	****	2.753	***
	Pde3a	1.637685	ns	2.36	**	2.1	*
	Snca	2.863292	***	23.9	****	2.10443	*
Fibrotic Genes	Col11a1	3.240188	****	8.76	***	2	*
	Col1a1	6.175983	****	0.1	*	0.53	ns
	Col3a1	6.653946	****	0.07	*	0.13	****
	Ctgf	3.743725	****	0.46	ns	1.877	*
	Dcn	0.644718	ns	0.21	**	0.094	*
	F2r	2.613409	****	1.96	ns	2.055	ns
	Fn1	5.051019	****	1.08	ns	0.0782	*
Signal Transduction Genes	Adra1a	2.529959	***	23.9	****	1.497	ns
	Adra1b	2.529959	**	2.05	***	1.28612	ns
	Adra1d	2.529959	***	21.87	****	2.038	ns
	Adrb1	1.76	**	1.25	****	2.46	ns
	Adrb2	2.52	***	32.97	****	4.2363	****
	Mapk1	1.053645	ns	1.6	*	1.48	ns
	Mapk8	2.178454	**	5	****	1.2	ns
	Pde3b	2.539398	**	74.77	****	1.54	ns
	Pde5a	2.52	***	9.57	****	2.68	*
	Pde7a	2.571273	***	9.78	****	2.68	*

3.5.6. Fibrotic genes were differentially regulated in in vivo *and* in vitro *cardiac disease models*

Cardiac fibrosis post-I/R injury in the heart is dependent on cardiac fibroblasts activation *in vivo* [44]. Our analyses showed that changes in decorin (Dcn), collagen, type XI, alpha 1 (Col11a1) and coagulation factor II (thrombin) receptor (F2r) were similar *in vitro* and *in vivo* compared to the controls. All other genes were differently regulated *in vitro* and *in vivo*. In particular, collagen, type III, alpha 1 (Col3a1) and fibronectin 1 (Fn1) were upregulated *in vivo* and downregulated in both *in vitro* models. Collagen, type I, alpha 1 (Col1a1) and connective tissue growth factor (Ctgf) were upregulated *in vivo* and in hCSs but downregulated in mCSs (table 1). The difference in expression of fibrotic genes could be because it requires 3 d to fibrotic genes to fully express themselves following a hypoxic event in *in vivo*. Therefore I/R CSs may require additional time for the reoxygenation to induce the fibrotic response *in vitro* [19].

Our analyses of fibrotic genes after DOX treatment showed that the expression of Dcn and Col3a1 was downregulated in both hCSs and mCSs compared to their respective controls, whereas Col11a1, Ctgf and F2r were upregulated in both hCSs and mCSs in comparison to their controls. Unlike other fibrotic genes Col1a1 and Fn1 showed differential expression in mCSs and hCSs where both the genes were upregulated in mCSs and are downregulated in

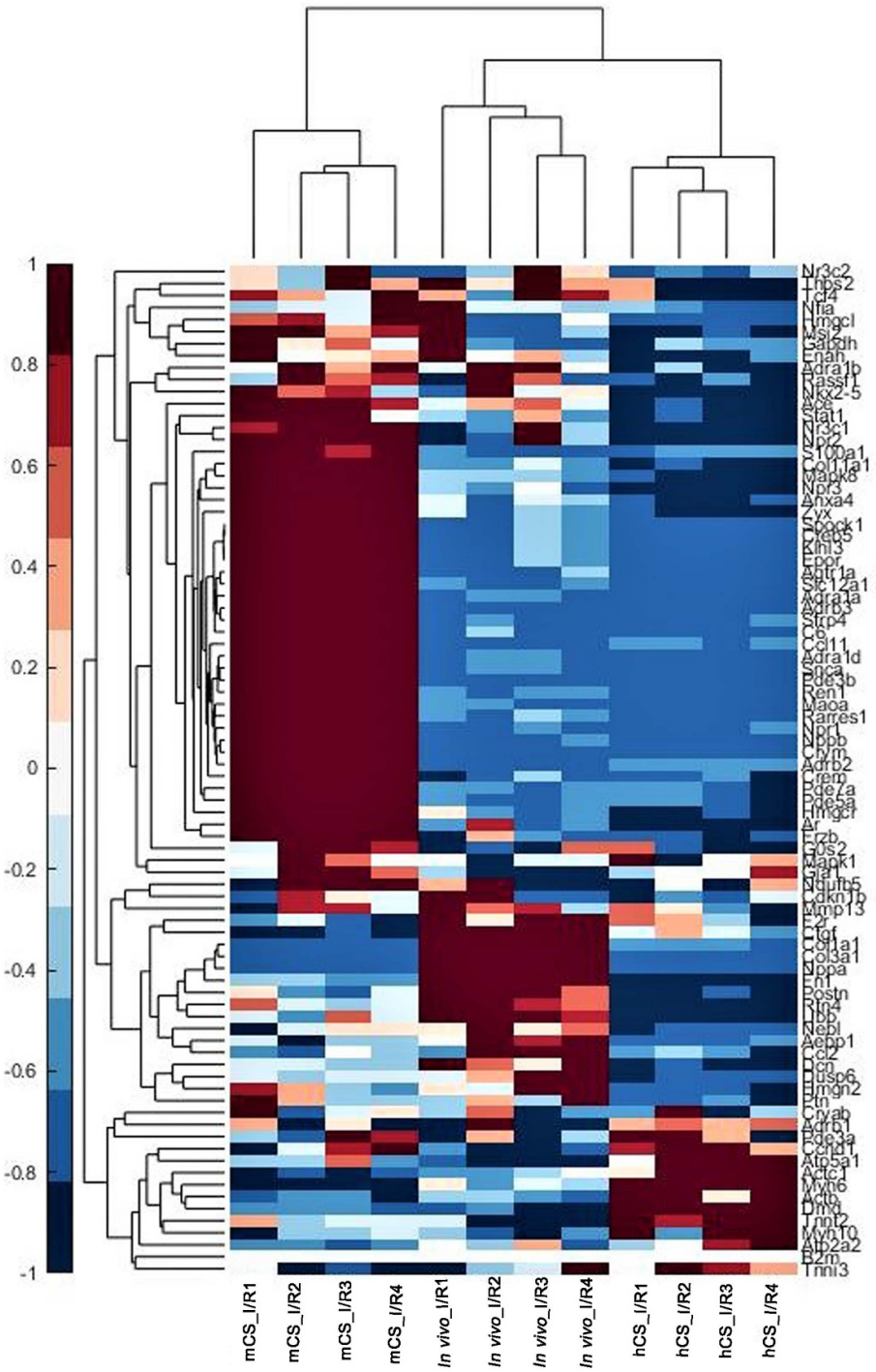

Figure 8. Difference in expression of cardiac genes in *in vivo* and *in vitro* models of myocardial I/R injury. Heat map of the differential expression of cluster of genes obtained after principal component analyses in mCSs, *in vivo* mouse and hCSs moving from right to left. The color bar on the right side indicates the intensity of expression.

hCSs compared to their respective controls (table 2). Fibrosis caused by DOX was also confirmed by a previous study where expression of osteopontin a cytokine that is involved in reconfiguration of the extracellular matrix and contributes to cardiomyocyte death in H9c2 rat heart derived embryonic myocytes and adult mice hearts was studied which is consistent with our study [45].

3.5.7. Signal transduction genes were consistently regulated in I/R and DOX CSs

Adrenergic receptors, mitogen-activated protein kinases and phosphodiesterases play a critical role in the regulation of signal transduction in the myocardium [42, 46, 47]. All of these genes were upregulated in both *in vitro* and *in vivo* following injury. These include: (a) adrenergic receptors, such as alpha 1a

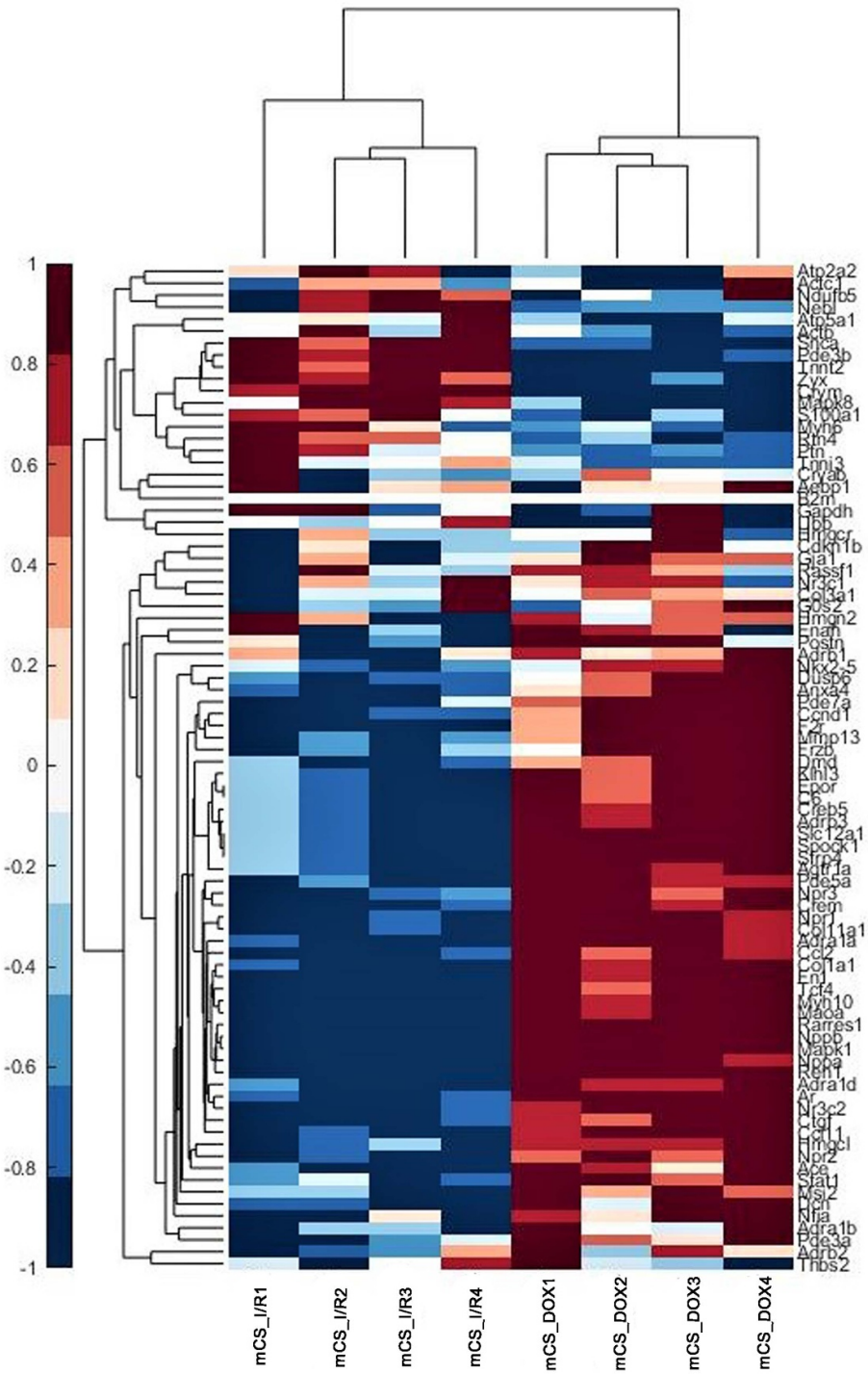

Figure 9. Difference in expression of cardiac genes in *in vitro* I/R and DOX mCSs. Heat map of the differential expression of cluster of genes obtained from principal component analyses in mCSs, comparing I/R and DOX-mediated response from right to left. The color bar on the right side indicates the intensity of expression.

(Adra1a), alpha 1b (Adra1b), alpha 1d (Adra1d), beta 2 (Adrb2) and beta3 (Adrb3); (b) mitogen-activated protein kinases, such as Mapk1 and Mapk8 and (c) phosphodiesterase enzymes, such as 3B cGMP-inhibited (Pde3b), 5 A cGMP-specific (Pde5a) and 7a (Pde7a) (table 1).

All the signal transduction genes analyzed in our study (such as, Adra1a, Adra1b, Adra1d, Adrb2, Adrb3, Mapk1, Mapk8, Pde3b, Pde5a and Pde7a) were upregulated in both mCSs and hCSs compared to controls (table 2). These results are consistent with others, suggesting that in response to the DOX-mediated cardiotoxicity the expression of signal transduction proteins such as adrenergic receptor proteins, Map kinases and phosphodiesterases is increased to induce a cardioprotective effect [48, 49].

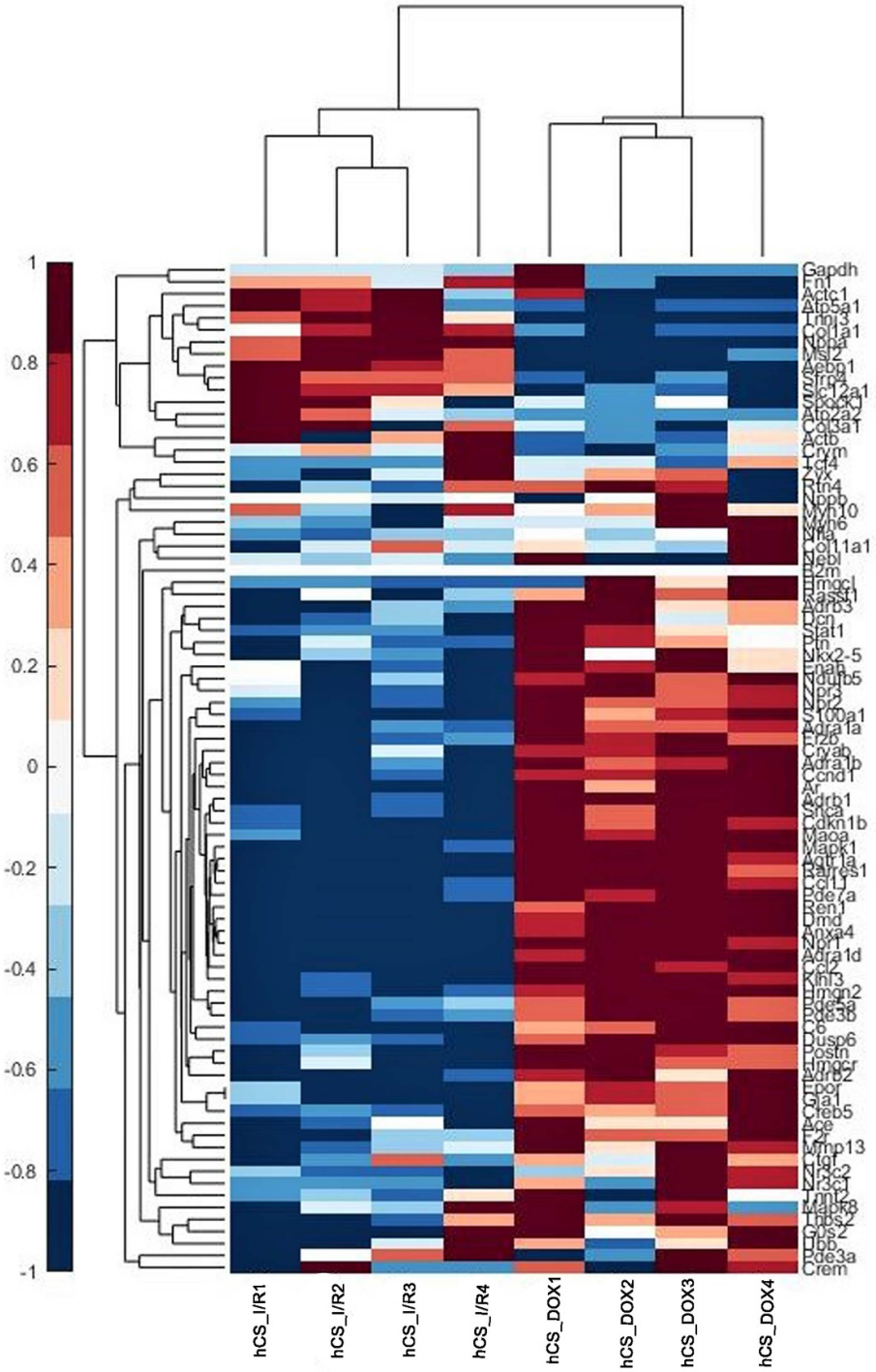

Figure 10. Difference in expression of cardiac genes in *in vitro* I/R and DOX hCSs. Heat map of the differential expression of cluster of genes obtained from principal component analyses in hCSs, comparing I/R and DOX-mediated response from right to left. The color bar on the right side indicates the intensity of expression.

4. Discussion

Myocardial I/R and drug-induced cardiac damages are the primary causes of all the deaths that occurred due to CVD across the globe [17, 18]. There is an urgent need for advanced *in vitro* human heart models that can closely recapitulate these complex scenarios. More specifically, clinically relevant approaches that can easily and directly translated into clinical trials are required to combat these major killers [17]. In this study, we showed that *in vitro* CSs from human cells can serve as a clinically relevant approach to model several aspects of myocardial I/R injury typical of an MI event and drug-induced cardiac damage in humans. These include changes in cell viability and death, contractile function and gene expression levels. In order to replicate *in vivo* conditions typical of an MI event in *in vitro* CSs, we exposed CSs to pathophysiological changes in O_2. Given the novelty of this approach, we developed our own model

Table 2. Expression of cardiovasular genes following DOX-treatment. Relative expression of sacromeric genes, calcium transporting genes, cell cycles genes, apoptotic genes, fibrotic genes and signal transduction genes in *in vitro* mCSs, and *in vitro* hCSs. The blue colour represents downregulated genes and red represents the upregulated genes. Unpaired t-test, $p > 0.05$ = ns, $p < 0.05$ = *, $p < 0.01$ = **, $p < 0.001$ = *** and $p < 0.0001$ = ****, ($n = 4$).

		QPCR analyses of cardiovascular genes to evaluate the DOX-induced cardiac damage			
		In vitro mCSs		*In vitro* hCSs	
Classification of genes	Genes	Fold change	*P*-value	Fold change	*P*-value
Sarcomeric Genes	Actc1	0.05	**	0.13	*
	Myh10	12.85	****	6.35	****
	Myh6	0.03	**	0.75	ns
	Tnni3	0.04	**	0.025	**
	Tnnt2	0.01	***	0.15	**
Calcium Transporting Genes	Atp2a2	0.04	****	0.07238	****
	Atp5a1	0.12	****	0.19	****
Cell Cycle Genes	Ccnd1	11.64	****	7.99	****
	Rarres1	75.14	****	9.63	****
Cardiac Remodelling Genes	Ace	8.19	****	2.56	*
	Mmp13	4.72	****	3.96	***
	Ren1	44.24	****	6.63	****
Apoptotic Genes	Anxa4	10.04	****	12.05	****
	Ccl2	4.32	****	6.88	****
	Maoa	36.59	****	5.26	****
	Nppa	2.614748	*	0.016	ns
	Nppb	79.05	****	0.33	ns
	Npr1	43.41	****	9.32	****
	Pde3a	4.37	****	2.56	***
	Snca	12.38333	****	7.56	****
Fibrotic Genes	Col11a1	14.77	****	2.43	**
	Col1a1	3.516667	****	0.13	ns
	Col3a1	0.06	*	0.11	*
	Ctgf	4	****	2.47	**
	Dcn	0.74	ns	0.11	***
	F2r	7.7966	****	4.33	***
	Fn1	9.5767	****	0.06	ns
Signal Transduction Genes	Adra1a	44.24	****	3.61	***
	Adra1b	3.79	****	3.76	****
	Adra1d	37.03	****	15.35	****
	Adrb1	2.31	****	4.302	****
	Adrb2	36.36	****	7.987	ns
	Mapk1	10.37	****	4.74	ns
	Mapk8	4.89	****	1.19	****
	Pde3b	32.38	****	3.77	****
	Pde5a	17.71	****	4.676	**
	Pde7a	15.15	****	9.43	****

of myocardial I/R injury by exposing CSs incubated with reversible hypoxic dye to normoxic conditions followed by hypoxic conditions followed by normoxic conditions (figure 2). The overtime reversible changes in fluorescence of the hypoxic dye showed that the CSs very well sense the pathophysiological alterations in O_2 concentration to mimic *in vivo* I/R. For the evaluation of drug-induced cardiac damage, CSs were incubated with DOX. Sebastio *et al* [15] in their recent study showed that post I/R injury in both *in vitro* and *in vivo* conditions, cardiomyocytes die and cannot form spheroid cultures. We observed a similar response following I/R conditions *in vitro* for cardiomyocytes, fibroblasts and endothelial cells, as demonstrated by our toxicity ratio and 3D rendering analyses of I/R CSs (figures 3 and 5, video 2). Our results of I/R mediated toxicity are also consistent with a previous study focusing on *in vitro* and *in vivo* necrosis caused by I/R, demonstrated by flouresecent staining for cell death and infarct size, respectively [50]. Similarly, Maillet *et al* [51] reported cell death in human iPSC-derived cardiomyocytes following DOX treatment, also consistent with our DOX-induced cell death results. Our toxicity ratio and 3D rendering analyses of DOX-treated CSs follow our previous studies focused on the response of cardiomyocytes, endothelial cells and fibroblasts in CSs (figures 4 and 6, video 3) [8]. We report that cell death in I/R and DOX CSs is also correlated with a reduction in fractional shortening and contraction frequency in DOX CSs, with the greatest inhibitory effects in I/R CSs (figure 7, videos 4, 5 and 6).

Our results showing that fractional shortening and contractile reductions in *in vitro* CSs could reflect the scenario observed in *in vivo* functional cardiomyopathies, as measured by ultrasound techniques as fractional shortening, contraction frequency and ejection fraction [52–55]. Our qPCR analyses demonstrated that changes in mRNA expression levels of cardiac damage-related genes measured *in vivo* were recapitulated for a variety of gene in I/R CSs (figure 8, table 1). For this study, *in vivo* I/R ventricular samples were isolated from adult male murine hearts that underwent a temporary LAD ligation, whereas control animals received a sham procedure only. These tissues were then used to compare the changes measured in *in vitro* models. Among the genes that presented a similar trend *in vivo* and *in vitro*, we report the downregulation in Actc1 mRNA expression levels following I/R injury (table 1), which is consistent with a previous study by Zimmermann *et al* [56], in a pig *in vivo* model. It was also reported that Actc1 was severely downregulated following oxidative stress in a mouse model of heart failure [24]. In our study we also measured a decrease in Myh6 in I/R CSs compared to control cultures, which is consistent with another study reporting a similar trend in both non ischaemic and ischaemic cardiomyopathy of a non-failing adult human heart [25]. Myh6 was also shown to be downregulated following the establishment of heart failure and left ventricular pressure overload in rabbits [26]. The upregulation of Myh10 we measured in CSs was consistent with what reported in rats post MI injury [27]. In another study, Wang *et al* [23] showed that Tnni3 is downregulated in mice two days post MI, which is consistent with our findings. The downregulation in Tnni3 and Tnnt2 was also linked to necrosis [22] and metabolic inhibition [57, 58]. In terms of calcium transporters Atp2a2 [33] and Atp5a1 [32, 59], they were both downregulated in I/R CSs compared to control cultures, consistent with another study conducted in mice [23]. Regarding changes in cell cycle related genes, Chen *et al* [60], showed that the Ccnd1 levels were increased in both neonatal mice and their cell cultures post MI, supporting our results. Similarly, Ccnd1 expression levels increased in adult T-box20 double transgenic mice following MI compared to α-Myosin Heavy Chain MerCreMer single transgenic mice as controls [61]. Another gene regulating cell cycle is Rarres1, a retinoic acid receptor, which was reported to be upregulated in unstable carotid endarterectomy plaque, consistent with our findings [62]. Among the several signal transduction genes we measured, phosphodiesterases, Map kinases and adrenergic receptors were previously reported to be upregulated post injury *in vivo*, which is again consistent with our study [63]. Among the apoptotic genes considered, Anxa4 was previously reported to be upregulated following hypoxic conditions *in vitro*, similar to what we reported in this study [64]. Similarly, another study by Korkmaz-Icöz *et al* [41] reported similar changes in apoptotic and fibrotic genes with our results.

When we analyzed changes in gene expression of DOX CSs, these showed a similar response as of I/R CSs. In particular, sarcomeric genes, such as Actc1, Tnni3, Tnnt2 and Myh6 were downregulated and Myh10 was upregulated compared to their respective controls (table 2). This is consistent with previously reported DOX-induced cardiac damage studies [28–30]. Our analyses of calcium transporting genes was also consistent with studies reporting reduced expression of Atp2a2 and Atp5a1 following DOX treatment [34]. We reported an upregulation of Ccnd1 and Rarres1 following DOX treatment, consistent with previous studies [36, 37]. Genes correlated with cardiac remodeling, such as Ace, Mmp13 and Ren1 were overexpressed in response to DOX treatment, typical of DOX- mediated myocardial damage [30, 39, 40]. We also observed that most of the apoptosis regulating genes are upregulated following DOX treatment compared to controls in both mCSs and hCSs, consistent with previous studies [30]. Signal transduction related genes were all upregulated in both mCSs and hCSs compared to controls suggesting consistency of our *in vitro* model with previous studies (table 2) [48, 49].

Previous studies using 3D *in vitro* cardiac models have been reported to study I/R and drug-induced damage on the heart [2, 65]. However, the majority of these studies lack a thorough recapitulation of features typical of the human heart in terms of cell composition and pathophysiological O_2 concentrations. More importantly, these studies only recapitulated the hypoxic event, without any analysis of the reoxygenation effects. To our knowledge, our study using *in vitro* CSs is the only one that deeply looked into these features by overcoming previous limitations. In this study, we have generated our CS models by using the three major cell types (cardiac myocytes, endothelial cells and fibroblasts), which were then used to recapitulate more clinically relevant aspects of an MI event. In particular, in our I/R injury we have used pathophysiological concentrations of O_2 (0% and 5%) to mimic *in vivo* I/R. However, it is important to highlight that our model may still lack important features of the *in vivo* MI event and the factors that elucidate pharmacokinetic and pharmacodynamic effects of a drug. The difference in behaviour of some of the genes in *in vivo* and *in vitro* could be linked to the fact that in *in vivo* there are several additional factors that influence the disease progression other than the confounding cell types we have in our *in vitro* CS models [1, 66]. In particular, in order to fully recapitulate the increase in expression levels of fibrotic genes measured *in vivo* (3 d following the hypoxic event), I/R CSs may require additional time for the reoxygenation to induce the fibrotic response observed *in vitro* and it may be used to discern between early and late effects of an MI event, given

the right conditions. Moreover, differences in gene expression levels between mCSs and hCSs could be species-specific [9, 67]. It is critical to acknowledge the limitations of our models and the fact that not all genes were upregulated and downregulated similarly *in vitro* and *in vivo*. One of these limitations is the absence of blood, blood derived cells and their effects on the myocardium, such as platelets, macrophages and other blood cells, all critical for the release of vasoconstrictive and proinflammatory agents typical of the myocardial I/R injury and DOX-induced cardiac damage *in vivo* [68]. Another important consideration is the fact we did not measure nor change the pH and calcium concentration to pathophysiological levels in I/R CSs [1]. This is due to the intrinsic static nature of our model, and future studies integrating I/R and DOX CSs in dynamic conditions may develop new approaches integrating the use of platelets and changes in pH and calcium concentrations *in vitro*. For instance, state-of-the-art microfluidics devices and bioprinting technology could be explored for the generation of high-throughput assays using I/R and DOX CSs and dynamic culture conditions mimicking blood flow.

5. Conclusion

Our study has presented for the first time a direct comparison between *in vivo* myocardial I/R injury and *in vitro* biofabricated CSs models that mimic features typical of MI. The cardiac damage observed in *in vivo* and *in vitro* demonstrated by our gene expression analyses of I/R CSs makes them suitable models to study myocardial damage following I/R injury and advanced alternatives to using animals for studies focusing on MI damage by using human cells in 3D *in vitro* cultures. Moreover, cardiac damage induced by DOX showed that our CS model is a multifaceted model that can be also used to test drug induced cardiac effects, including safety of drugs for patients. To our knowledge, this is the only *in vitro* 3D model able to mimic so many features typical of a damaged heart tissue following I/R injury, allowing the study of pathophysiological conditions, including the use of drugs in patients. This study has the potential to advance the field of cardiac tissue engineering for the biofabrication of novel *in vitro* cardiac models by better recapitulating the complex pathophysiology typical of a heart attack compared to other existing models.

Data availability statement

The data that support the findings of this study are available upon reasonable request from the authors.

Acknowledgments

Poonam Sharma was supported by University of Newcastle with UNIPRS and UNRS Central & Faculty School (UNRSC5050) scholarships. Laura A Bienvenu is supported by a National Heart Foundation (NHF) of Australia Postdoctoral Fellowship; Xiaowei Wang is supported by an NHF Future Leader Fellowship and a Baker Fellowship. Carmine Gentile was supported by a UTS Seed Funding, Catholic Archdiocese of Sydney Grant for Adult Stem Cell Research and a University of Sydney/Sydney Medical School Foundation Cardiothoracic Surgery Research Grant. A special thanks to Prof Louise Cole (UTS, Sydney) and to Dr Imala Alwis (Heart Research Institute, Sydney) for their assistance with confocal microscopy imaging.

Ethical statement

In vitro mCSs were generated under our approved protocol number RESP_17/55 from the Animal Ethics Committee at the Northern Sydney Local Health District St Leonards, NSW, Australia. *In vivo* animal procedures were performed under the approved protocol number E/1950/2019/B from Molecular Imaging and Theranostics Laboratory, Baker Heart and Diabetes Institute, Melbourne, Australia.

Conflicts of interest

The authors declare no conflict of interest.

ORCID iD

Carmine Gentile https://orcid.org/0000-0002-3689-4275

References

[1] Sharma P *et al* 2021 *Small* **17** 2003765
[2] Richards D J *et al* 2020 *Nat. Biomed. Eng.* **4** 446–62
[3] Ojha N *et al* 2020 *Myocardial Infarction, in StatPearls* (Treasure Island, FL: StatPearls Publishing)
[4] Kunecki M *et al* 2017 *Postepy Hig. Med. Dosw.* **71** 20–31
[5] Neri M *et al* 2017 *Mediators Inflammation* **2017** 7018393
[6] Ferlay J *et al* 2021 *Int. J. Cancer* **149** 778–89
[7] Soares R O S *et al* 2019 *Int. J. Mol. Sci.* **20** 5034
[8] Polonchuk L *et al* 2017 *Sci. Rep.* **7** 7005
[9] Chen T *et al* 2018 *Regen. Eng. Transl. Med.* **4** 142–53
[10] Kofron C M *et al* 2017 *J. Physiol.* **595** 3891–905
[11] Gentile C 2016 *Curr. Stem Cell Res. Ther.* **11** 652–65
[12] Zuppinger C 2019 *Front. Cardiovasc. Med.* **6** 87
[13] Veldhuizen J *et al* 2019 *J. Biol. Eng.* **13** 29
[14] Mills R *et al* 2020 *Nat. Biomed. Eng.* **4** 366–7
[15] Sebastiao M J *et al* 2020 *Transl. Res.* **215** 57–74
[16] Keeley T P *et al* 2019 *Physiol. Rev.* **99** 161–234
[17] Polonchuk L *et al* 2021 *Biofabrication* **13** 045009
[18] Sharma P *et al* 2021 *J. Vis. Exp.* **167** e61962
[19] Figtree G A *et al* 2017 *Cells Tissues Organs* **204** 191–8
[20] Bienvenu L A *et al* 2020 *Circ. Res.* **127** 1211–3
[21] Ziegler M *et al* 2018 *Eur. Heart J.* **39** 111–6
[22] Park K C *et al* 2017 *Cardiovasc. Res.* **113** 1708–18
[23] Wang Y *et al* 2018 *Acta Cardiol. Sin.* **34** 175–88
[24] Angelini A *et al* 2020 *FASEB J.* **34** 2987–3005
[25] Kittleson M M *et al* 2005 *Physiol. Genomics* **21** 299–307
[26] James J *et al* 2010 *J. Mol. Cell. Cardiol.* **48** 999–1006
[27] Wan W *et al* 2014 *Appl. Physiol. Nutr. Metab.* **39** 226–32
[28] Lenčová-Popelová O *et al* 2014 *PLoS One* **9** e96055

[29] Adamcova M *et al* 2019 *Int. J. Mol. Sci.* **20** 2638
[30] Boucek R J Jr *et al* 1999 *J. Mol. Cell. Cardiol.* **31** 1435–46
[31] Inesi G *et al* 2008 *Biochem. Biophys. Res. Commun.* **369** 182–7
[32] Ni R *et al* 2016 *Diabetes* **65** 255–68
[33] Lipskaia L *et al* 2014 *Biochim. Biophys. Acta* **1843** 2705–18
[34] Zhang Y *et al* 2014 *Cell Biochem. Biophys.* **70** 1791–8
[35] Lafontant P J *et al* 2006 *Heart Failure: Molecules, Mechanisms and Therapeutic Targets: Novartis Foundation Symposium* (Hoboken, NJ: Wiley Online Library) vol 274 pp 196–207 discussion 208–13, 272–6
[36] Haybar H *et al* 2021 *Jundishapur J. Chronic Dis. Care* **10** e112413
[37] Ma X *et al* 2020 *Sci. Adv.* **6** eaay2939
[38] Evans S *et al* 2020 *Sci. Rep.* **10** 14129
[39] Sobczuk P *et al* 2020 *Heart Fail. Rev.* **27** 295–319
[40] Sun X *et al* 2021 *Evidence-Based Complementary Altern. Med.* **2021** 6659676
[41] Korkmaz-Icöz S *et al* 2015 *J. Diabetes Res.* **2015** 396414
[42] Rose B A *et al* 2010 *Physiol. Rev.* **90** 1507–46
[43] Sergeeva I A *et al* 2013 *Biochim. Biophys. Acta* **1832** 2403–13
[44] Fu X *et al* 2020 *Front. Physiol.* **11** 416
[45] Schunke K J *et al* 2013 *J. Cell. Physiol.* **228** 2006–14
[46] Lohse M J *et al* 2003 *Circ. Res.* **93** 896–906
[47] Zhao C Y *et al* 2016 *J. Mol. Cell. Cardiol.* **91** 215–27
[48] Fajardo G *et al* 2006 *J. Mol. Cell. Cardiol.* **40** 375–83
[49] Prysyazhna O *et al* 2016 *J. Biol. Chem.* **291** 17427–36
[50] Hwang I-C *et al* 2018 *Hypertension* **71** 1143–55
[51] Maillet A *et al* 2016 *Sci. Rep.* **6** 25333
[52] Smiseth O A *et al* 2016 *Eur. Heart J.* **37** 1196–207
[53] Gnyawali S C *et al* 2010 *J. Vis. Exp.* **41** e1781
[54] Al-Biltagi M *et al* 2012 *ISRN Pediatr.* **2012** 870549
[55] Mitry M A *et al* 2016 *Int. J. Cardiol. Heart Vasc.* **10** 17–24
[56] Zimmermann M *et al* 2017 *Oncotarget* **8** 60809–25
[57] Hessel M H *et al* 2008 *Exp. Mol. Pathol.* **85** 90–95
[58] Rains M G *et al* 2014 *Clin Intervention Aging* **9** 1081–90
[59] Sommakia S *et al* 2017 *J. Mol. Cell. Cardiol.* **113** 22–32
[60] Chen Z *et al* 2017 *Cardiovasc. Res.* **113** 620–32
[61] Xiang F L *et al* 2016 *Circulation* **133** 1081–92
[62] van der Pouw Kraan T C *et al* 2010 *BMC Genomics* **11** 388
[63] López-Neblina F *et al* 2006 *J. Surg. Res.* **134** 292–9
[64] Vicic N *Exp. Cell. Res.* **340** 283–94
[65] Shen S *et al* 2021 *Biomed. Pharmacother.* **133** 110990
[66] Lindsey M L *et al* 2018 *Am. J. Physiol. Heart Circ. Physiol.* **314** H812–38
[67] van der Velden J *et al* 2019 *Physiol. Rev.* **99** 381–426
[68] Ziegler M *et al* 2019 *Cardiovasc. Res.* **115** 1178–88